Near ground results of the CO-SLIDAR C_n^2 profiler

C Robert[1], J-M Conan[1], L M Mugnier[1] and J-M Cohard[2]

[1] ONERA - The French Aerospace Lab F-92322 Châtillon, France

[2] Laboratoire LTHE, 70 rue de la Physique 38400 Saint Martin d'Hères, France

E-mail: clelia.robert@onera.fr

Abstract. CO-SLIDAR jointly uses the slopes and scintillation indices from a double source recorded with a Shack-Hartmann (SH) wavefront sensor which leads to a robust C_n^2 profile restoration. This technique coupled to a 0.35-m telescope in the mid-IR has provided horizontal C_n^2 profiles over 2.7 km with a 300 m resolution. The SH wavefront sensor data revealed a very good fit of the spatial spectra of the phase to the Kolmogorov model, and of the scintillation distributions to the small perturbation regime as well. Quantitatively the inversion of the measurement covariances allows us to retrieve the C_n^2 profile with small error bars and stable structure. These C_n^2 distributed estimations are comparable with the averaged C_n^2 measurements from scintillometers set in parallel.

1. Introduction

The development of C_n^2 profile measurement is flourishing in the astronomy domain. In the past years, several techniques have been developed, based on the analysis of the beam coming from a single or binary star. These techniques consist in analysing the fluctuations of intensity (scintillation) or those of the wavefront angle of arrival. To measure the C_n^2 profile in the whole atmospheric column, ONERA developed the CO-SLIDAR technique based on a Shack-Hartmann (SH) wavefront sensor [1]. The joint use of correlations of slopes and of scintillation, both measured on a binary source with a Shack-Hartmann, allows CO-SLIDAR to combine sensitivity to both low (close) and high altitude (far) layers.

In astronomical instrumentation, the knowledge of the C_n^2 profile is a key element to design and to evaluate the performance of future wide-field adaptive optics systems (WFAO) [2]. In this perspective, recent CO-SLIDAR experiments in the visible at the Observatoire de la Côte d'Azur (France) have measured C_n^2 profiles (with error bars) over 17 km of atmosphere with a resolution of 600 m. These C_n^2 profiles were compared successfully to those calculated from the re-analysis of meteorological data [3]. The CO-SLIDAR technique is of course applicable to oblique or horizontal paths provided one stays in the Rytov regime. In practice, limitations appear for horizontal 100-m paths in the surface layer where turbulence intensity is the highest, which leads to a saturation effect of scintillation indices in the visible range and thus prevents the inversion of the C_n^2 distribution. Longer distances are possible using the CO-SLIDAR in the thermal infrared domain for km paths. Thus our IR Shack-Hartmann [4] was used to provide distributed C_n^2 values along a horizontal path near the Earth surface. These C_n^2 horizontal profiles can be further used to estimate sensible and latent heat surface fluxes at parcel scale which is relevant for climate, hydrological, and agronomics studies.

As the CO-SLIDAR principle and the on-sky results obtained at Observatoire de la Côte d'Azur have been presented in [3], the proceeding will focus on the near ground results.

2. Multi-instrument campaign for near ground C_n^2 profiles

A field experiment named AMOSC was conducted at the Centre de Recherche Atmosphérique (CRA) in Lannemezan (France) to first optically calibrate CO-SLIDAR horizontal C_n^2 profiles. This experiment was conducted in fall 2012 (ONERA with French labs LTHE, INRA, CESBIO). The SH ($\lambda = 3.8$ μm) was installed on the CRA roof, aiming at a vertical double halogen source placed 2.7 km apart in the church tower of the Campistrous village. In addition, 3 scintillometers (using a diode at $\lambda = 0.9$ μm as a source) were co-aligned with this line of sight, that was 22 meters in average above ground (see Fig. 1). The CO-SLIDAR profiles were to be compared with the C_n^2 values estimated from the scintillometers. Each one had been configured with a specific configuration of apertures - with their own weighting function - to highlight different parts of the path. We got finally 21 days of SH data synchronized with the scintillometers and micro-meteorological data. Data processing is still in progress and we present first encouraging results in this paper.

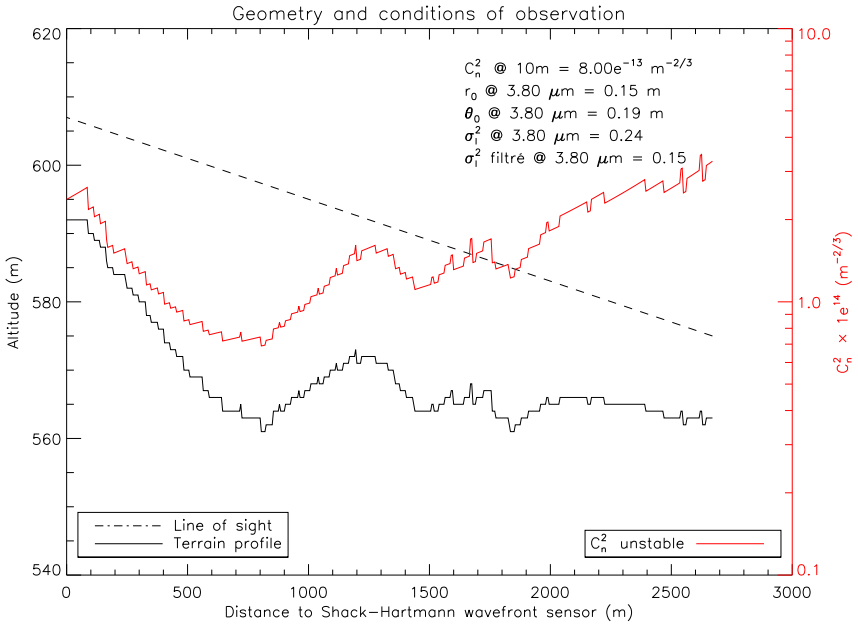

Figure 1. Terrain profile (black) and line of sight (dashed). Model of atmospheric boundary layer C_n^2 (h) profile (red) according to C_n^2 $(h_0 = 10m) \times h^{-4/3}$, corresponding to diurnal conditions (unstable), with h being the height of the line of sight. Derived turbulence parameters are given at $\lambda = 3.8$ μm.

3. CO-SLIDAR principle: direct problem, inversion and error bars

We currently only exploit correlations of x-slopes, of y-slopes and of scintillation to speed up the computing time since coupling between x and y-slopes are weaker. Correlations are averaged over all pairs of subapertures with given separation and represented as auto- or cross-correlation map as it relates to one or two sources. Then, one pixel of these six maps is stacked into a vector $\mathbf{C_{mes}}$. The latter is related to the discretized C_n^2 profile at different distances z, denoted $\mathbf{C_n^2}$, by the following linear relationship:

$$\mathbf{C_{mes}} = M\mathbf{C_n^2} + \mathbf{C_d} + \mathbf{u}. \tag{1}$$

M is the matrix of the weighting functions for slopes and for scintillation [3] derived here for a spherical wave since sources are at a finite distance. Because of detection noises, the pseudo-measurements $\mathbf{C_{mes}}$ are biased with the averaged correlations of these noises $\mathbf{C_d}$. As we estimate the correlations from a finite number of frames, $\mathbf{u}$ represents a Gaussian convergence noise.

The $\mathbf{C_n^2}$ profile is retrieved by minimizing the Maximum *A Posteriori* (MAP) metric composed of the Maximum Likelihood criterion with a spike preserving regularization $J_{\mathrm{p}}\left(\mathbf{C_n^2}\right)$ (white L1L2 [5]) assuming independent layers, which is relevant for horizontal profiles:

$$J_{\mathrm{MAP}}\left(\mathbf{C_n^2}\right) = \left(\mathbf{C_{mes}} - \mathbf{C_d} - M\mathbf{C_n^2}\right)^{\mathrm{T}} C_{\mathrm{conv}}^{-1}\left(\mathbf{C_{mes}} - \mathbf{C_d} - M\mathbf{C_n^2}\right) + J_{\mathrm{p}}\left(\mathbf{C_n^2}\right). \tag{2}$$

The covariance matrix of the convergence noise $C_{\rm conv} = \langle \mathbf{u}\mathbf{u}^{\rm T} \rangle$, is approximated with the pseudo-measurements correlations. In addition, the diagonal values of matrix $\left(M^{\rm T} C_{\rm conv}^{-1} M\right)^{-1}$ represent an upper bound of the variances of the $\mathbf{C_n^2}$ estimates [3], from which 3σ error bars on the reconstructed profile are readily computed.

4. Resolution in distance of the horizontal C_n^2 profiles

Since our IR Shack-Hartmann looks at a double source with an angular separation $\theta = 60$ arc second and has 5 subapertures in its pupil diameter D, we can retrieve at least 5 layers up to the maximal distance of triangulation $H_{max} = D/\theta = 1.3$ km thanks to the cross-correlations of slopes and of scintillation. Beyond the triangulation range H_{max} we will also estimate the profile from the auto-correlations of scintillation averaged on every single source and involving several subaperture baselines sampling the structure of the farthest weighting functions of scintillation (Cf. Fig. 2). Note the FWHM[1] of the 3 functions at $z = 1.7, 2.0$ and 2.3 km span over 2 subapertures allowing to exploit their mutual scintillation. In the following we will estimate the C_n^2 profiles on a grid of 8 layers regularly spaced along the path.

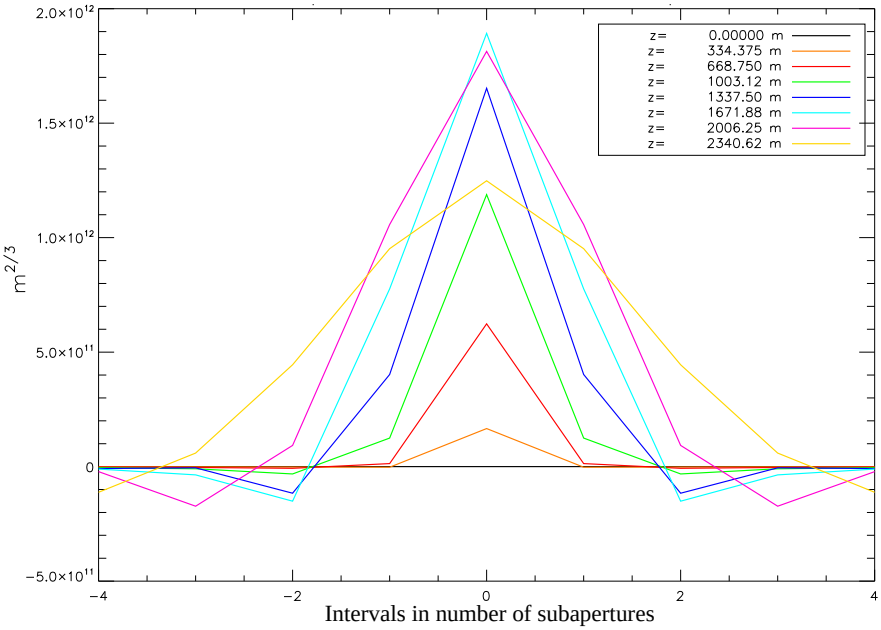

Figure 2. Cross sections of the scintillation weighting functions varying the distance z to the SH.

5. Shack-Hartmann data quality check

Before performing inversion of (1) to estimate the C_n^2 profile from the slopes and scintillations, we need to check if the data respect the model assumptions, namely Kolmogorov and the weak perturbation regime. To do so, we extract slopes and scintillation from the SH image spots (25×25 pixels) in moving windows of 7×8 pixels, and we check the turbulence statistics from the two kinds of data. From the slopes we compute the Zernike coefficient variances. It shows a Kolmogorov turbulence without noticeable outer scale effect (see Fig. 3). We validate the weak perturbation regime using intensity fluctuations, by fitting a log-normal distribution (see Fig 4) and estimating the Rytov variance. The latter was found to be far below 0.3, validating the hypothesis of weak perturbations at $\lambda = 3.8$ μm. Derived log-amplitude from intensity is in excellent agreement with the Gaussian law. The correlation maps in Fig. 5 present the expected patterns: The cross-correlation map of scintillation (Fig. 5a) and that of the slopes (Fig. 5d) shows peaks of correlation in the direction of the source alignment, representing the turbulent layers' signatures up to H_{max}. Last but not least the auto-correlation map of scintillation (Fig. 5b) covers 2 subapertures, and this signal is useful to estimate the $\mathbf{C_n^2}$ values beyond H_{max}. All these verifications confirm the data consistency with the model assumptions.

[1] Full Width at Half Maximum.

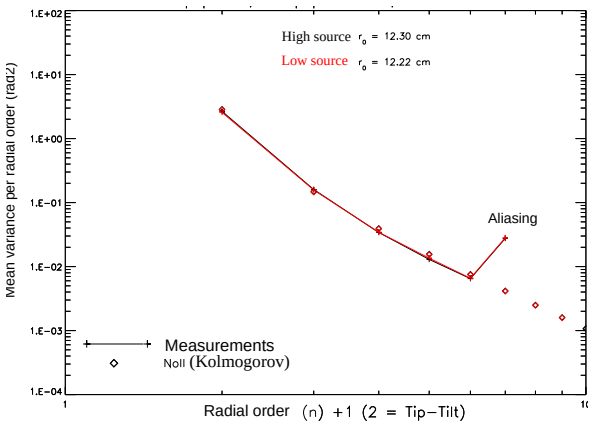

Figure 3. Mean Zernike variances over 1 min. (8520 wavefronts) on 14/09/12 at 14:19.

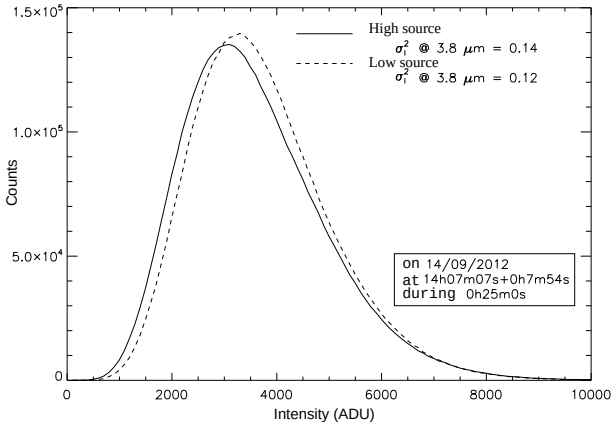

Figure 4. Log-Normal intensity distributions of the high and low sources.

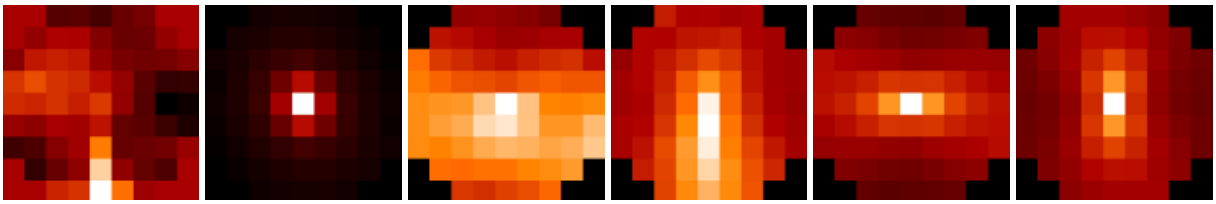

Figure 5. Correlation maps from scintillation and slopes measured with the mid-IR SH. Example of 1−min. records (8520 frames) at 14:15 on 14/09/12 . From left to right: (a) cross-correlation of scintillation between the sources, (b) auto-correlation of scintillation on each source, (c) cross-correlation (two sources) of y-slopes, (d) cross-correlation (two sources) of x-slopes, (e) auto-correlation (one source) of y-slopes, (f) auto-correlation (one source) of x-slopes.

6. Reconstruction of the horizontal C_n^2 profiles

We present on Fig. 6 one example of C_n^2 profile obtained from 1 minute SH data. The structure of the profile is clearly visible on the 8 reconstructed layers with small error bars (convergence noise). There are three significant layers with C_n^2 ranging $3-5\ 10^{-14}\ m^{-2/3}$. Two of them are placed at the sight line ends (CRA roof and the village) and one thick layer is located between 900 m and 1200 m. Very low C_n^2 values are observed elsewhere, especially the one almost null located at 1500 m. The horizontal lines show the integrated C_n^2 measured from the scintillometers (dashed) and synthesized (continuous) from the estimated C_n^2 profile. Their length illustrates the effective footprint of the scintillometers weighting functions.

CO-SLIDAR C_n^2 profiles are now compared with C_n^2 values integrated from the scintillometers. A good match is obtained in the first part of the path (magenta) but for the other two parts (black, blue) the trend is opposite between integrated C_n^2 synthesized with CO-SLIDAR and that measured from scintillometers. Even if the orders of magnitude are correct, these discrepancies require further investigations.

In any case, r_0 and scintillation indices from the CO-SLIDAR C_n^2 profiles fit well those measured directly for the sequence of a dozen minutes (see Figs. 7-8). A 4% error is obtained for r_0, while a 10% error is obtained for the scintillation. This means that unsteady conditions cannot be involved in the discrepancies mentioned. Finally, Fig. 9 shows a day and night turbulence variation as expected and a stable structure of the C_n^2 profiles.

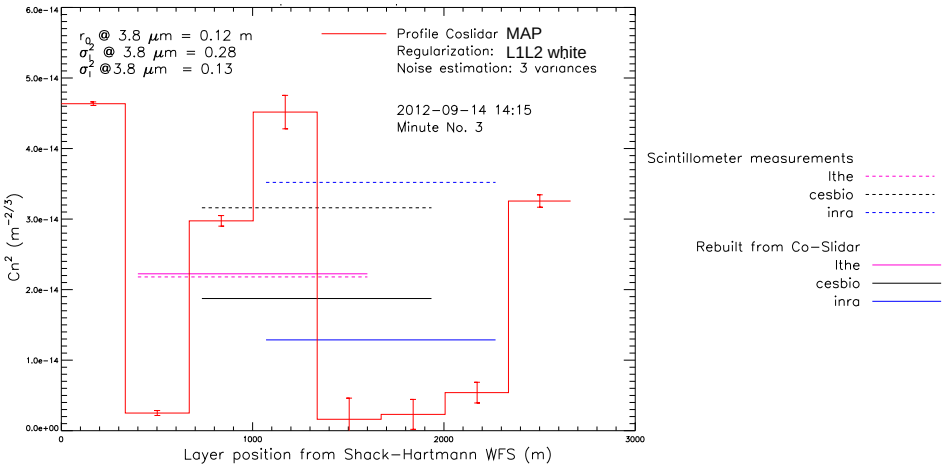

Figure 6. Comparison between C_n^2 profiles and integrated C_n^2 values from scintillometers on 14/09/12.

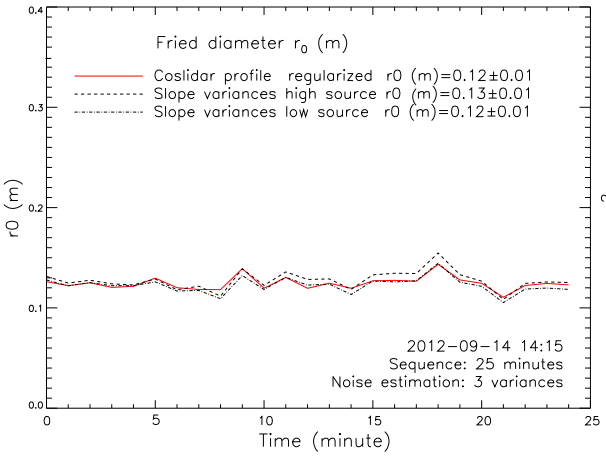

Figure 7. Fried parameter variation along time.

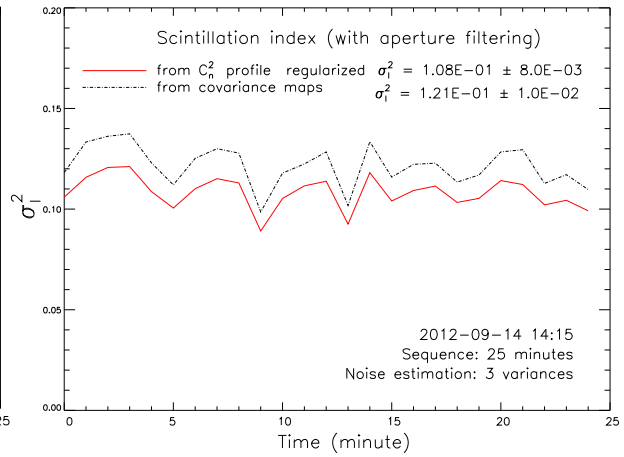

Figure 8. Scintillation index variation along time.

7. Conclusion and perspectives

Near ground CO-SLIDAR in the mid-IR using a 0.35-m telescope provides C_n^2 profiles over 2.7 km with 300 m resolution. The joint use of slopes and scintillation leads to robust C_n^2 profile restoration with small error bars, even beyond the triangulation range thanks to scintillation. r_0 and scintillation indices from the CO-SLIDAR C_n^2 profiles fit well those measured directly from the slopes and scintillation variances. C_n^2 CO-SLIDAR profiles have been compared with C_n^2 values integrated from the scintillometers, both showing a day and night turbulence variation. But reverse order between both distributions require further investigations. To sort it out we have planned inter-comparison campaigns on homogeneous and restrained heterogeneous surfaces. CO-SLIDAR development is set out to build a lighter device to bring it outdoors easily and estimate in addition to the C_n^2 profile the transverse wind profile, perpendicular to the sight line. The motivation of this work is to obtain inputs for sensible and latent heat flux calculation.

CO-SLIDAR can also provide relevant inputs for site characterization, for design and performance evaluation of WFAO ELT instruments that will include multi-WFS. The need of an external vertical C_n^2 distribution to calibrate the internal low resolution C_n^2 profile is envisaged. Position with respect to other astronomical C_n^2 profilers is yet to be analyzed during inter-comparison campaigns [6]. Anyway whatever the application whether it be water management in environment or astronomic instrumentation, CO-SLIDAR C_n^2 profiles can help the forecast of atmospheric surface parameters and optical turbulence.

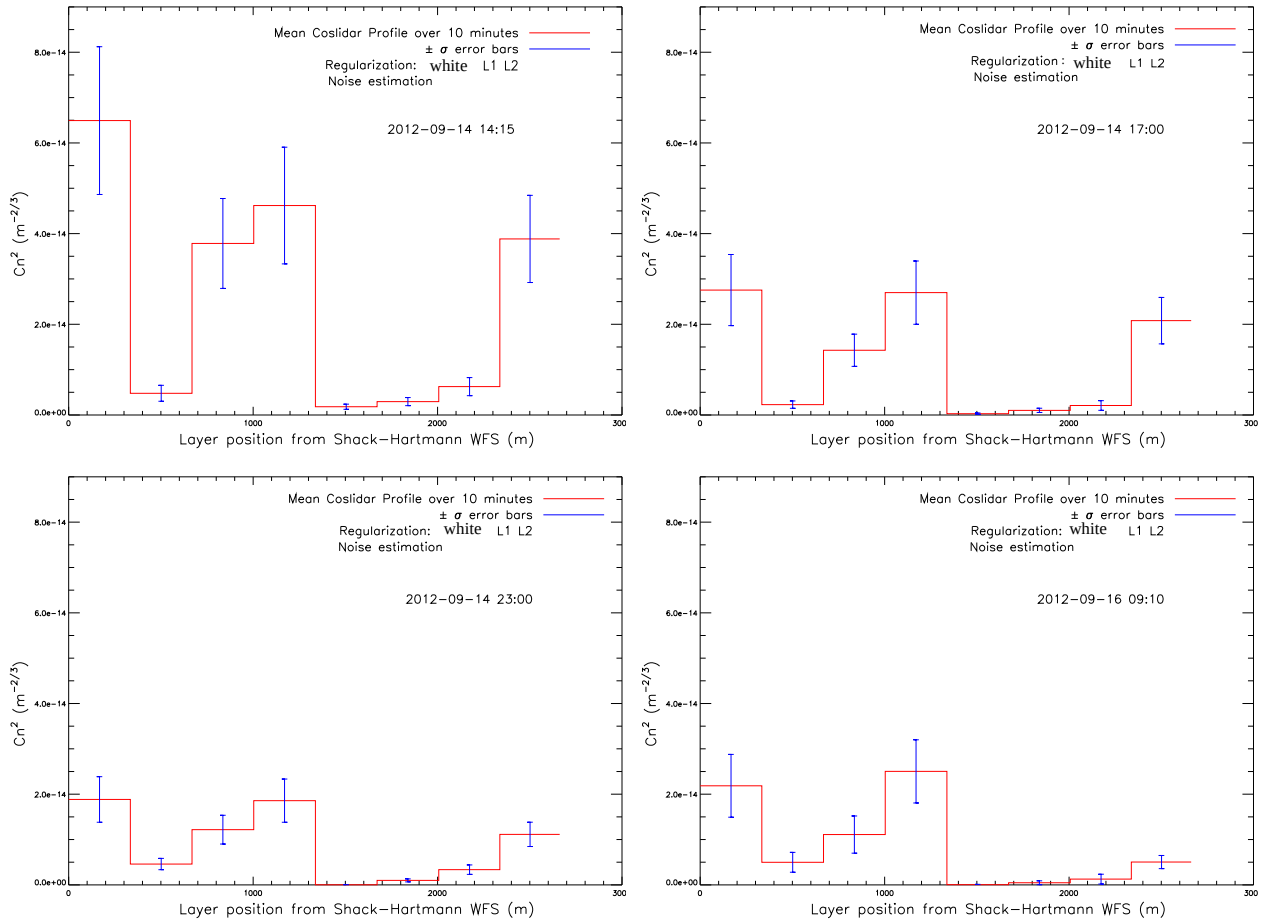

Figure 9. Mean C_n^2 profiles averaged over 10 minutes (red) and their standard deviations (blue). Variation during afternoon, evening (upper graphs), night, morning (lower graphs) on consecutive and sunny dates.

Acknowledgments

The authors wish to acknowledge assistance from PhD J Voyez and training student Y Tellier, technical work by F Mendez and B Fleury, fruitful discussions with M-T Velluet, V Michau and N Védrenne, then financial support from CNRS and ONERA. We would also like to thank J-P Lagouarde who initially proposed this study. We express our gratitude to M Irvine and A Brut for their dedicated assistance during the observations.

References

[1] Védrenne N, Michau V, Robert C and Conan J-M 2007 *Optics Letters* **32** 2659–2661

[2] Costille A and Fusco T 2011 *Second International Conference on Adaptive Optics for Extremely Large Telescopes.* vol 1 p 78 URL `http://ao4elt2.lesia.obspm.fr/spip.php?article603`

[3] Voyez J, Robert C, Conan J-M, Mugnier L M, Samain E and Ziad A 2014 *Opt. Express* **22** 10948–10967

[4] Robert C, Michau V, Fleury B, Magli S and Vial L 2012 *Opt. Express* **20** 15636–15653 URL `http://www.opticsexpress.org/abstract.cfm?URI=oe-20-14-15636`

[5] Meimon S, Mugnier L M and Le Besnerais G 2009 *J. Opt. Soc. Am. A* **26** 108–120

[6] Masciadri E, Rousset G, Fusco T, Basden A, Bonifacio P, Fuensalida J, Robert C, Sarazin M, Wilson R and Ziad A 2013 Conference date: May 2013, Florence